ADVANCED FUNCTIONAL MATERIALS
www.afm-journal.de

Plasmon-Enhanced Fluorescent Sensor based on Aggregation-Induced Emission for the Study of Protein Conformational Transformation

*Yanyun Cui, Chang Yuan, Hongwei Tan, Zhanbin Zhang, Yijing Jia, Na Na, and Jin Ouyang**

The alteration in protein conformation not only affects the performance of its biological functions, but also leads to a variety of protein-mediated diseases. Developing a sensitive strategy for protein detection and monitoring its conformation changes is of great significance for the diagnosis and treatment of protein conformation diseases. Herein, a plasmon-enhanced fluorescence (PEF) sensor is developed, based on an aggregation-induced emission (AIE) molecule to monitor conformational changes in protein, using prion protein as a model. Three anthracene derivatives with AIE characteristics are synthesized and a water-miscible sulfonate salt of 9,10-bis(2-(6-sulfonaphthalen-2-yl) vinyl)anthracene (BSNVA) is selected to construct the PEF–AIE sensor. The sensor is nearly non-emissive when it is mixed with cellular prion protein while emits fluorescence when mixed with disease-associated prion protein (PrP^{Sc}). The kinetic process of conformational conversion can be monitored through the fluorescence changes of the PEF–AIE sensor. By right of the amplified fluorescence signal, this PEF–AIE sensor can achieve a detection limit 10 pM lower than the traditional AIE probe and exhibit a good performance in human serum sample. Furthermore, molecular docking simulations suggest that BSNVA tends to dock in the β-sheet structure of PrP by hydrophobic interaction between BSNVA and the exposed hydrophobic residues.

1. Introduction

The alteration in protein conformation not only affects the performance of its biological functions, but also leads to a large variety of protein-mediated diseases including Alzheimer's disease (AD), Parkinson's disease (PD), type II diabetes, prion disease, etc.[1] Developing an effective method for monitoring the changes of protein conformation is very important for the diagnosis and treatment of protein conformation disease. At present, several techniques have been successfully used in monitoring protein conformational changes, such as nuclear magnetic resonance (NMR), circular dichroism (CD), Fourier transform infrared spectroscopy, atomic force microscopy, scanning electron microscopy (SEM), fluorescence spectroscopy, positron emission tomography, and surface-sensitive measurement techniques.[2] Among them, fluorescence methods have received increasing attention owing to the advantages of rapidity, simplicity, low cost, and high sensitivity.[3] Some types of fluorophores have been reported to be able to bind to oligomers or fibrils to present different fluorescence emissions, such as congo red, thioflavin T, 1-anilino-naphthalene-8-sulfonate, rhodamine derivatives, and quantum dots.[2a,d,4] However, these conventional dyes suffer from several drawbacks including low specificity, insufficient sensitivity, and false-positive response.[5] In addition, protein transformation involves multiple processes, and most fluorescent molecules are not able to detect intermediates, hence being unsuitable for kinetic studies.[6] Moreover, these fluorophore molecules usually go through serious self-quenching when they are concentrated or bounded to biomacromolecules due to the aggregation caused quenching (ACQ) effect.[7]

Aggregation-induced emission (AIE) molecules are a class of fluorophores that are non-emissive at dissolved state, but become highly fluorescent emission at aggregated state.[8] They can effectively conquer the ACQ effect of conventional dyes.[9] In addition, they have several advantages, including the large Stokes' shift, strong photostability, and high signal-to-noise ratio.[7a,10] Based on the unique properties of AIE molecules, they are widely used in the detection of metal ions and small molecules, stimuli response, fluorescence imaging, etc.[11] More importantly, the AIE molecules are very sensitive to the changes of microenvironment, so they are especially suitable for monitoring the change progress of protein conformational. Tang et al. synthesized 1,2-bis[4-(3-sulfonatopropoxyl)phenyl]-1,2-diphenylethene, which has good AIE properties and has been successfully implemented in monitoring the unfolding process of human serum albumin.[12] Since then, AIE molecules have stepped onto the stage of protein conformation monitoring. Subsequently, a large number of AIE molecules

Y. Cui, C. Yuan, Prof. H. Tan, Prof. Z. Zhang, Y. Jia, Prof. N. Na, Prof. J. Ouyang
Key Laboratory of Theoretical and Computational Photochemistry
Ministry of Education
College of Chemistry
Beijing Normal University
Beijing 100875, China
E-mail: jinoyang@bnu.edu.cn
The ORCID identification number(s) for the author(s) of this article can be found under https://doi.org/10.1002/adfm.201807211.

DOI: 10.1002/adfm.201807211

© 2019 WILEY-VCH Verlag GmbH & Co. KGaA, Weinheim

are synthesized and used to detect the fibrillation or unfolding process of insulin, erythropoietin, α-synuclein, etc.[5,6,13] However, most AIE molecules have poor water solubility which limits their practical applications. In addition, the hydrophobic interaction between AIE molecules and proteins is the main detection mechanism, which leads to poor binding selectivity. Furthermore, the low binding efficiency of recognition assay limits the sensitivity. Therefore, it is necessary to develop new AIE sensors with high sensitivity and specificity in aqueous solution for biological macromolecules detection.

Signal amplification is a promising approach to obtain high sensitivity sensors.[14] The localized surface plasmon resonance of metal nanoparticles (NPs) can greatly amplify the electromagnetic (EM) field around them, which in turn enhances the surrounding fluorescence to achieve plasmon-enhanced fluorescence (PEF).[15] PEF can improve the fluorescence performance of fluorescent molecules and the detection sensitivity of target molecules. At present, a variety of fluorescent molecules have achieved fluorescence enhancement through the PEF effect, including porphyrin dyes, cyanine dyes, nucleic acid stain, and fluorescein.[16] However, these conventional dyes usually undergo serious self-quenching when they are concentrated or bounded to biological macromolecules due to the intermolecular π–π stacking interactions, which greatly limits their applications in biological macromolecular detection.[11c,17] In addition, they are not sensitive to the changes of microenvironment and cannot monitor biological processes such as protein conformation changes. Inspired by the advantages of PEF and AIE effects, we has designed to introduce the AIE molecules into PEF system, enabling the PEF sensor to show new potential in protein conformation monitoring and other biological processes.

In this work, a hybrid PEF–AIE sensor consisting of plasmonic Au@SiO_2 NPs coupled with AIE molecule was designed for monitoring protein conformational changes. First, three anthracene derivatives with different substituents were successfully designed and synthesized. All of them exhibited excellent AIE characteristics and self-assembly effects, especially the sulfonate salt of 9,10-bis[2-(6-sulfonatopropoxyl)naphthylethenyl] anthracene (BSNVA). Subsequently, BSNVA molecules were introduced into the PEF system by taking advantages of the specific recognition of protein by aptamer and the interaction between protein and BSNVA molecules. The Au@SiO_2 NPs can significantly enhance the fluorescence intensity of BSNVA molecules in solution. Although organic–inorganic hybrid sensors have been reported, the combination of AIE and PEF systems has been rarely reported.[11d,15a,18] By regulating the thickness of silicon shell, we successfully achieved the fluorescence enhancement of AIE molecules, which expands the application scope of PEF. Water-soluble AIE molecules have a lower background interference level in aqueous solutions than traditional dyes, which makes them more suitable for PEF system. This design can not only improve the performance of fluorescent molecule, but also overcome the disadvantage of self-quenching of traditional dyes. Compared with most previous methods, the new method in this paper constructed a turn-on and label-free fluorescence sensor by combining PEF and AIE. By means of the signal amplification, the PEF–AIE sensor exhibits outstanding sensitivity and selectivity for target protein detection. Furthermore, using prion protein (PrP) as the model, the PEF–AIE sensor is further applied to monitor the change of protein conformation. This strategy may serve as a common method for protein conformational transformation, which is of great importance to the diagnosis and treatment of protein-conformational diseases.

2. Results and Discussion

The preparation of the PEF–AIE sensor was illustrated in **Scheme 1**. First, we successfully synthesized a anthracene derivative of BSNVA. Good water solubility and low quantum yield in aqueous solution make BSNVA suitable for PEF sensor. Au nanocubes (Au NCs) coated with silica (Au@SiO_2) was

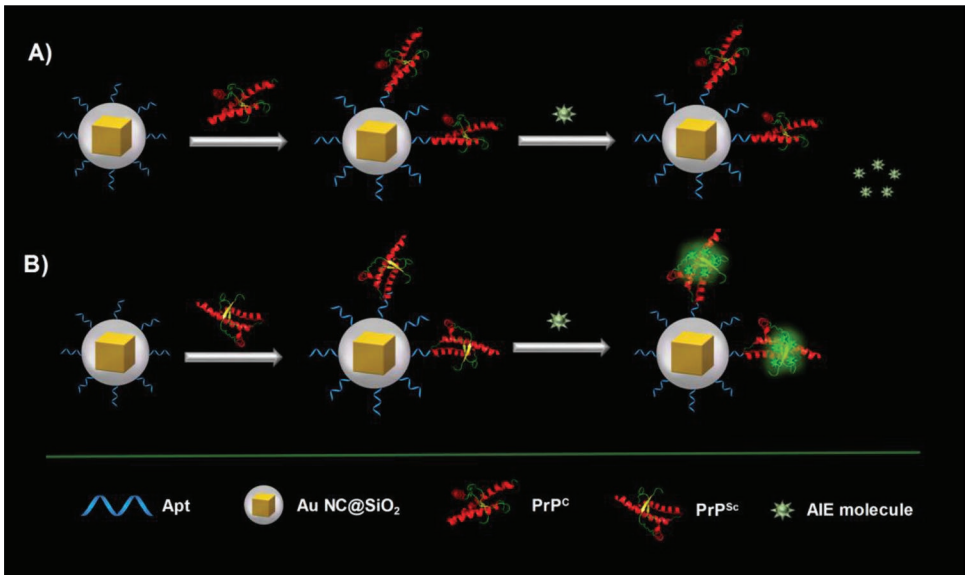

Scheme 1. Schematic illustration of PEF sensor based on AIE molecules for the detections of A) PrP^C and B) PrP^{Sc}.

© 2019 WILEY-VCH Verlag GmbH & Co. KGaA, Weinheim

selected as the PEF matrix, and BSNVA as fluorescence emitter was introduced into PEF system. The Au@SiO_2 NPs were further modified with aptamer to capture PrP in the solution. In the presence of cellular prion protein (PrP^C), BSNVA molecules are dispersed in water, as BSNVA is difficult to bind to PrP^C (Scheme 1A). Instead, with the introduction of disease-associated prion protein (PrP^{Sc}), the highly specific interactions between aptamer and PrP^{Sc} can promote the formation of Au@SiO_2-Apt-PrP^{Sc} complexes. At the same time, AIE molecules bind spontaneously to PrP^{Sc} through hydrophobic interactions, leading to an obvious fluorescence enhancement (Scheme 1B). Accordingly, changes in the conformation of PrP can be obtained by monitoring the variation of fluorescence intensity.

2.1. Synthesis and Characterization of Anthracene Derivatives

Anthracene and its derivatives are a typical class of AIE molecules due to their excellent optical properties and chemical stability.[19] Through the Witting–Horner reaction, three anthracene derivatives were designed and synthesized, namely BMNVA, BHNVA, and BSNVA (Scheme S1, Supporting Information). The general synthetic route is shown in **Figure 1**. The products and key intermediates are characterized by NMR and mass spectrometry (Figures S1–S5, Supporting Information). It is envisioned that BMNVA, BHNVA, and BSNVA will have AIE performances benefiting from the 9,10-anthylene core.[20] They have weak fluorescence in the dispersed state, because the vibration of 9,10-anthylene and rotation of aryl peripheries in the solution can dissipate excitation energy. However, an intensive fluorescence was observed in the aggregated state owing to the restriction of intramolecular motions (RIM), resulting in the blocking of the non-radiative decay channel.[21]

Furthermore, poor–good solvent systems were chosen to confirm their AIE characteristics. Tetrahydrofuran (THF)-H_2O mixed solvent was used to investigate the AIE characteristics of BMNVA. BMNVA showed weak fluorescence when dissolved in pure THF. However, with the addition of water, the fluorescence (FL) intensity gradually increased and reached the maximum value when the volume fraction of water (f_w) was 80%, and BMNVA emitted strong green light with the FL emission peak centered at 525 nm (**Figure 2**A,B). The absorption spectra of BMNVA in THF-water mixture are shown in Figure S6A in the Supporting Information, and the change trend is consistent with the FL spectra. The maximum absorption of BMNVA in THF is 418 nm. When the f_w reaches 60%, the absorption intensity at 418 nm disappears, while a weak band appears at 476 nm. When f_w is 80%, a remarkable absorption band at 476 nm represents the formation of BMNVA aggregates in suspensions. Similarly, the AIE performances of BHNVA were evaluated in the same mixed solvent. BHNVA exhibited weak fluorescence when completely dissolved in pure THF. However, the FL intensity of BHNVA increased dramatically upon increasing the f_w and reached the highest level when the volume of water was 70% (Figure 2C, D). As a sulfonate salt, BSNVA can dissolve in water and exhibits weak fluorescence. With the THF fraction (f_T) increasing, the FL intensity go up by 13.2-fold when the f_T is 80% (Figure 2E,F). As mentioned above, all three compounds have good AIE properties. In addition, BMNVA possesses solvatochromism characteristics, along with enhancement of the solvent polarities, and the emission bands redshift from 516 to 535 nm (Figure S6B, Supporting Information). The mechanical grinding and thermal stimulation make the luminous colors of the as-prepared powders convert between orange and green emission under UV light, which further enables BMNVA to be used on the eraser board (Figure S6C,D, Supporting Information).

Shape and size determine the physicochemical properties of materials, turning the shape control into a hot topic in material science.[22] Studies have shown that AIE molecules could self-assemble into various shapes. In this work, three anthracene derivatives with different substituents were synthesized and the solution evaporation approach was employed to prepare their self-assembled structures. The fluorescence microscopic images demonstrated that solution evaporation process led to the formation of aggregation into different shapes in the

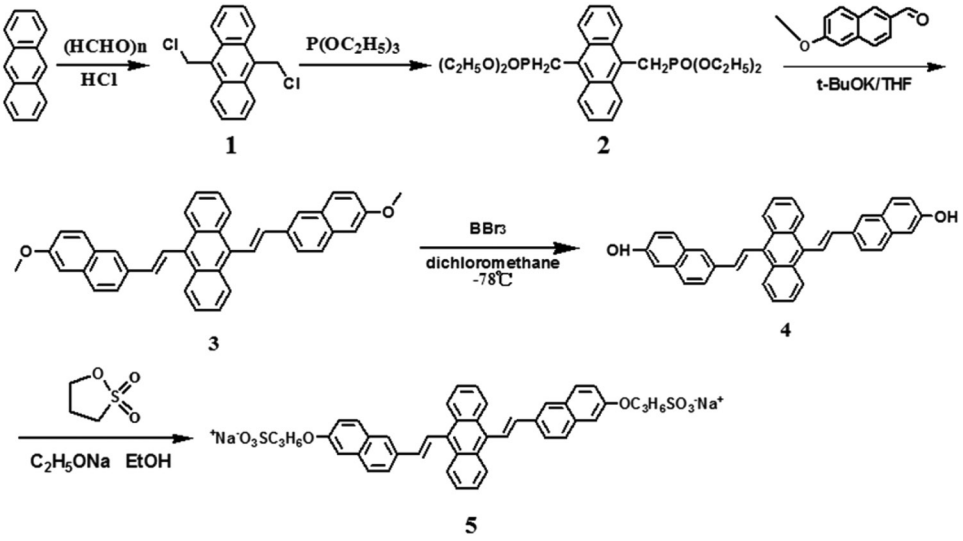

Figure 1. Synthesis routes of AIE molecules.

© 2019 WILEY-VCH Verlag GmbH & Co. KGaA, Weinheim

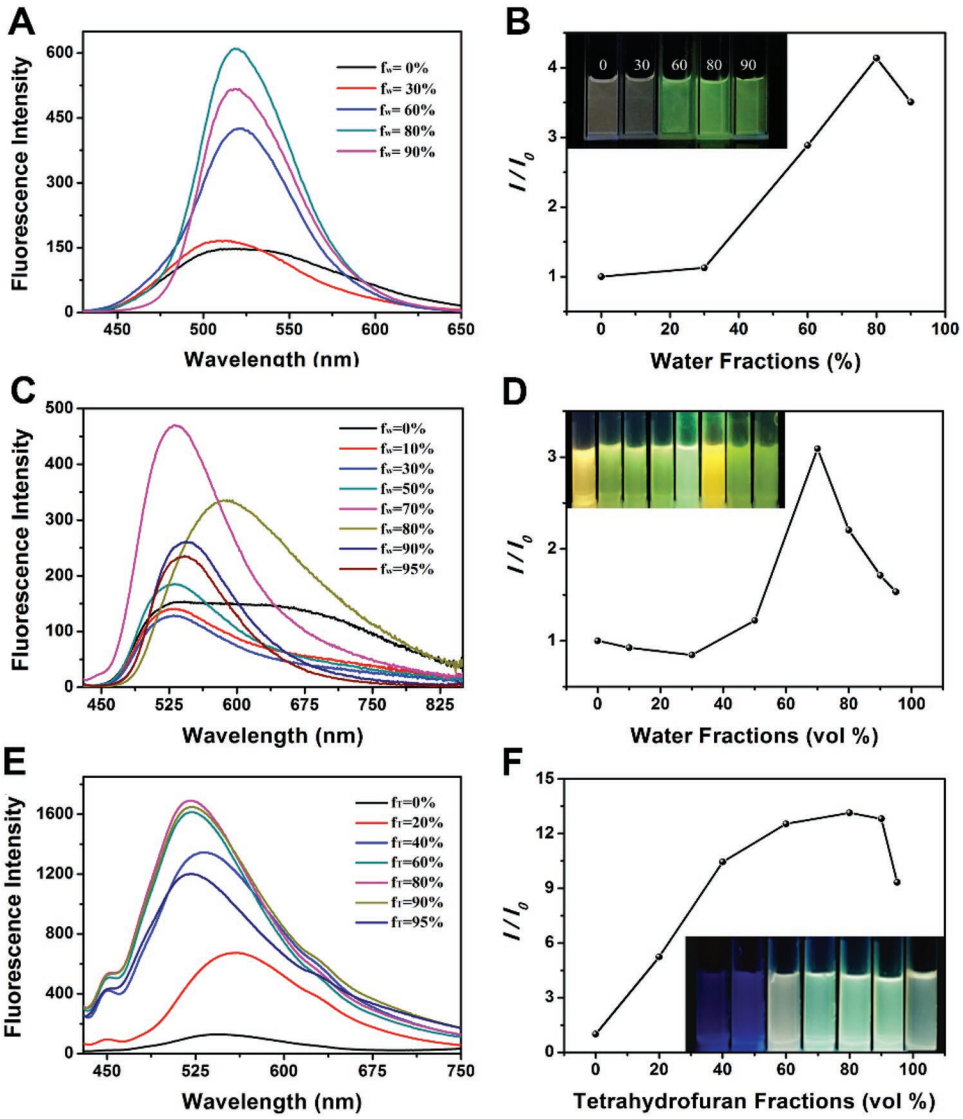

Figure 2. A) FL spectra and B) plot of relative FL intensity (I/I_0) of BMNVA in THF/water mixtures with different water fractions (f_w), where I_0 is the FL intensity in THF. C) FL spectra and D) plot of relative FL intensity (I/I_0) of BHNVA in THF/water mixtures with different f_w, where I_0 is the FL intensity in THF. E) FL spectra and F) plot of relative FL intensity (I/I_0) of BSNVA in THF/water mixtures with different THF fractions (f_T), where I_0 is the FL intensity in water. The inset photo shows the corresponding emission colors under UV illumination.

THF/water mixtures (**Figure 3**). BMNVA with methoxy group could assemble into irregular flake-like, needle-shaped, leaf-like, and xiphophyllous structures in the THF/water mixtures with f_w = 30%, 70%, 80%, and 90% (Figure 3A). In the same proportion of solvents, the compound BHNVA with hydroxyl appeared in needle-shaped, diamond-shaped, spherical, and blend shapes, respectively (Figure 3B). Similarly, sulfonate derivatives also exhibited excellent self-assembly performance. As displayed in Figure 3C, BSNVA forms green emission needles, and the length and width are different along with the increasing of f_T. In addition, the fluorescence microscopic images also describe the luminescence colors of different aggregates, such as diamond BHNVA emitting green fluorescence, while spherical BHNVA showing yellow emission. By comparing the fluorescence microscopy results of the three AIE molecules, it can be concluded that the introduction of different substituents to anthracene derivative can effectively change the self-assembly behavior of AIE compounds. The above results are consistent with the AIE properties of the three molecules, indicating that the change of luminescence properties of three AIE molecules are related to their self-assembly morphology and aggregation degree.

2.2. Fabrication of PEF–AIE Sensor

The enhanced local EM fields around plasmonic nanostructures can dramatically modify the optical properties of adjacent fluorescent molecules, known as PEF.[16a] PEF is considered as an attractive biosensing technique as it can improve detection sensitivity of target molecules. The plasmon metallic NPs are key factors in PEF because they can serve as antennas

© 2019 WILEY-VCH Verlag GmbH & Co. KGaA, Weinheim

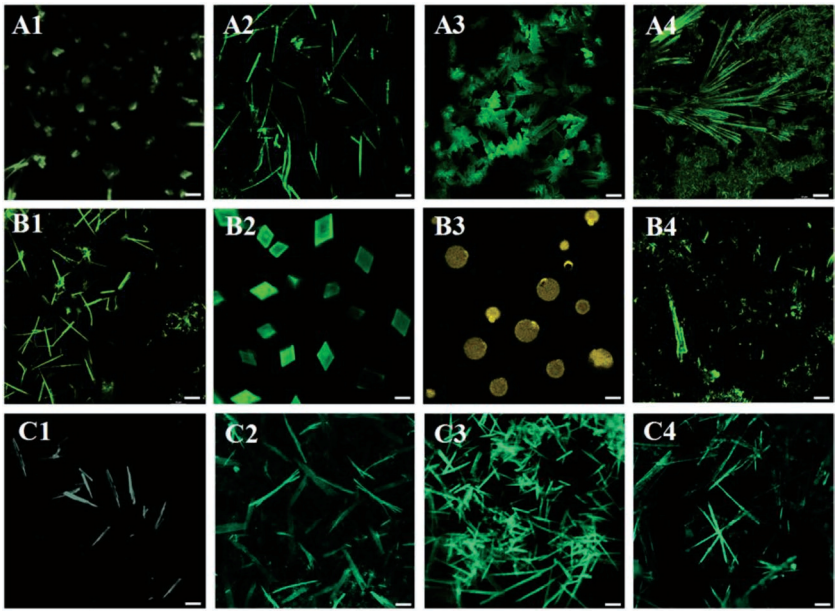

Figure 3. Fluorescence microscopy images of A) BMNVA, and B) BHNVA generated by evaporating suspensions of THF/water mixtures with f_w = 30%, 70%, 80%, and 90%, and C) BSNVA in THF/water mixtures generated the same way with f_T = 30%, 70%, 80%, and 90% .

providing enhanced EM field.[23] Au NCs, with multiple sharp corners and edges of "hot spots", are considered as suitable materials for PEF.[16d] In this work, Au NCs with an average diameter of about 50 nm were prepared by a seed-growth method, which possessed a surface plasmon absorption at 540 nm (**Figure 4**A,E). When the distance between the dyes and the metallic nanostructures is less than 10 nm, the fluorescence of dyes is quenched due to fluorescence resonance energy transfer.[24] Therefore, silica was chosen as the dielectric spacer to control the spacing distance, and an average thickness of the silica shell was about 15.7 nm (Figure 4B). Silica can easily be modified, providing convenience for the aptamer conjugation. Subsequently, Au NC@SiO_2 NPs was modified by $-NH_2$ groups and further connected to the aptamer. Compared with the Au NCs, there was a redshift in the plasmon absorption from 540 to 555 nm by a series of surface modifications, which was induced by the change of dielectric environment. However, the shape of the plasmon absorption of Au NC remained unchanged, suggesting that the functionalization process did not affect the morphology of the Au NCs (Figure 4C). Zeta potential measurements revealed that the potential changed after the modifications of $-NH_2$ and aptamer, and the corresponding potential values were respectively 28.1 and −10.7 eV (Figure 4D). In addition, the stability of Au@SiO_2-Apt NPs is estimated. Figures S7 and S8 in the Supporting Information show that the UV–vis spectrum and the size remain unchanged within 3 d, which confirms Au@SiO_2-Apt NPs are stable in the short term. Being a fluorescent nucleicacid stain for double-strand DNA, picoGreen (PG) was employed to further confirm the connection between the aptamer and Au NC@SiO_2 NPs. After removing unconnected aptamer by multiple washes, Au NC@SiO_2-Apt was incubated with the complementary DNA (cDNA) of Apt. As a result, a fluorescence emission of PG that gradually increased with the increase of cDNA was observed, indicating that the aptamer had been successfully conjugated to the surface of Au NC@SiO_2 (Figure S9, Supporting Information). The conjugation number of aptamer to Au NC@SiO_2 was calculated to be 409 ± 24 aptamer per Au NC@SiO_2 (Supporting Information).

The selection of fluorescent molecule is one of the factors to be considered in designing a PEF sensor. The spectral overlap between the plasmon resonance wavelength and the absorption or emission of the fluorophore influences the enhancement of the emission intensity.[25] BSNVA is selected as the signal molecule in this work, which possesses two negative charges, exhibiting good water solubility. More importantly, the emission wavelength of BSNVA is 540 nm, which completely overlaps with the plasma absorption of Au NCs (Figure 4E). Unlike traditional dyes, BSNVA shows the unique AIE properties that dissolve in aqueous solution with almost no luminescence, greatly reducing the interference of background fluorescence. Moreover, BSNVA is sensitive to hydrophobic environments, and its aromatic core can spontaneously bind to the hydrophobic region of PrP^{Sc} rich in β-sheet structure, hence switching on its light emission. In the enhancement system, Au NC@SiO_2-Apt can capture the PrP^{Sc} molecules in the solution through the specific binding of the Apt. At the same time, the BSNVA molecules are indirectly connected to the surface of the core–shell structure by hydrophobic interactions with PrP^{Sc}. Therefore, an obvious fluorescence enhancement of BSNVA is observed. As reported, the separation distance determined the overall PEF efficiency.[25] In order to achieve the optimal fluorescence enhancement, six thicknesses of the silica shell ranging from 8.1 to 41.6 nm were prepared (**Figure 5**A–F). The highest fluorescence enhancement for Au@SiO_2-Apt-PrP^{Sc}-BSNVA NPs when the silica shell thickness was 15.7 nm, which is 18.5 times higher than BSNVA (Figure 4F and Figure S10, Supporting Information). SiO_2-Apt-PrP^{Sc}-BSNVA NPs are used as control sample because they do not affect the fluorescence of dyes, hence serving as a common method to observe PEF.[16c,26]

2.3. PEF–AIE Sensor for Discrimination of PrP

Prion disease, also known as transmissible spongiform encephalopathy (TSE), is a fatal neurodegenerative disease caused by the infection of prion.[27] PrP^C and PrP^{Sc} are two isoforms of PrP, with the same amino acids sequence but different in conformation. PrP^{Sc} is considered as an early biomarker for prion disease, and the conversion of PrP^C to PrP^{Sc} is the mechanisms of TSE.[28] Therefore, the discrimination of two conformers of PrP is the premise of studying its conformational changes. PrP^C has a mainly α-helical structure, while PrP^{Sc} has a rich β-sheet structure.[29] It is hypothesized that the PEF–AIE sensor can be used to distinguish PrP^C and PrP^{Sc}, because BSNVA can bind to the grooves of β-sheet structures. To prove its feasibility,

© 2019 WILEY-VCH Verlag GmbH & Co. KGaA, Weinheim

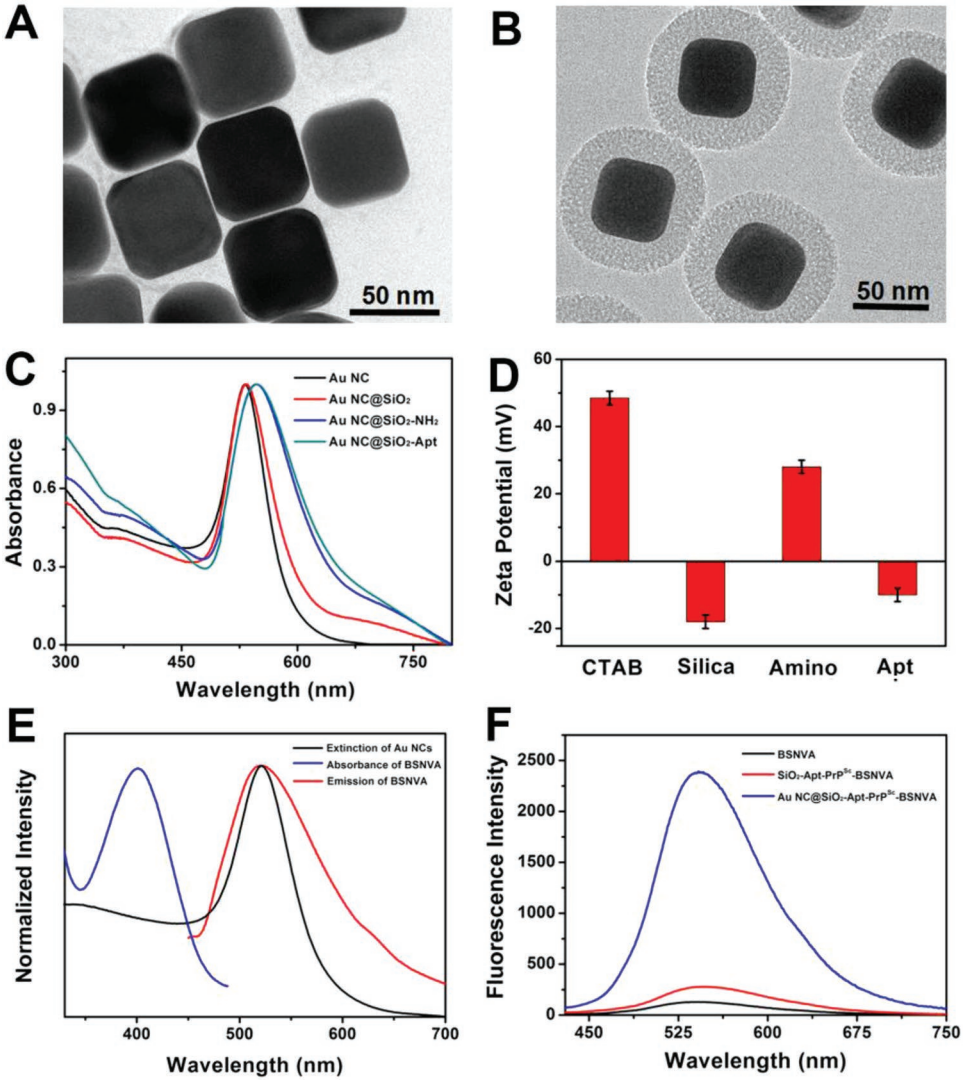

Figure 4. A) TEM image of Au NCs. B) TEM image of core–shell Au NC@SiO_2 NPs. C) UV–vis absorbance spectra of Au NCs, Au NC@SiO_2, Au NC@SiO_2-NH_2, and Au NC@SiO_2-Apt. D) Zeta-potential values of Au NCs coated with CTAB, silica shell, functionalized with the amino, and connected with Apt. E) The extinction spectrum of Au NCs, excitation, and emission spectra of BSNVA. F) FL spectra of BSNVA, SiO_2-Apt-PrP^{Sc}-BSNVA, and Au NC@SiO_2-Apt-PrP^{Sc}-BSNVA.

the FL responses of the PEF–AIE sensor to PrP^C and PrP^{Sc} were carried out. As shown in **Figure 6**A, BSNVA solution is almost non-emissive due to its excellent water solubility. After the addition of PrP^C, the solution of Au NC@SiO_2-Apt-PrP^C-BSNVA shows a weak fluorescence. PrP^C is positively charged, while BSNVA carries a negatively charged under neutral conditions, resulting in weak fluorescence due to a small amount of electrostatic adsorption.[30] However, the sensor is switched on when the PrP^{Sc} is added. At this point, PrP^{Sc} is negatively charged, which prevents BSNVA molecules from binding to PrP^{Sc} due to the electrostatic repulsion between the same charges.[31] However, the extended β-sheet structures of PrP^{Sc} allow BSNVA molecules accumulate on its surface through hydrophobic interaction, which limits the intramolecular motion and thus lits up the fluorescent signal of BSNVA. The Au NC@SiO_2-Apt-PrP^{Sc}-BSNVA and Au NC@SiO_2-Apt-PrP^C-BSNVA solutions in sunlight are transparent (Figure 6B). Under the ultraviolet irradiation, Au NC@SiO_2-Apt-PrP^C-BSNVA solution is almost non-emissive, while Au NC@SiO_2-Apt-PrP^{Sc}-BSNVA solution switches on green emission (Figure 6C). The large FL intensity differences between Au NC@SiO_2-Apt-PrP^C-BSNVA and Au NC@SiO_2-Apt-PrP^{Sc}-BSNVA, which indicates that the sensor can effectively distinguish PrP^{Sc} from PrP^C.

2.4. PEF–AIE Sensor for Monitoring the Conformational Change of PrP

The distinct fluorescence responses of AIE–PEF sensor in the presence of PrP^C and PrP^{Sc} prompted us to try to use it to monitor the conformational change process of PrP. PrP^C is stable under neutral pH and changes in conformational at low pH, resulting in the formation of PrP^{Sc}.[32] We dissolved PrP^C in a sodium acetate–acetic acid buffer (pH 4.0) and incubated it at 65 °C to achieve

© 2019 WILEY-VCH Verlag GmbH & Co. KGaA, Weinheim

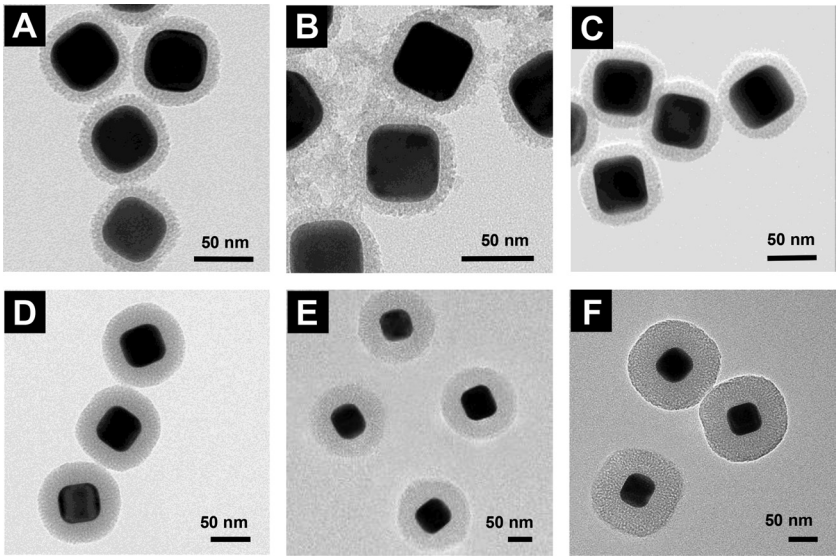

Figure 5. TEM images of Au NC@SiO_2 NPs with increasing silica shell thicknesses A) 8.1, B) 11.3, C) 15.7, D) 23.1, E) 34.5, and F) 41.6 nm.

the transformation from PrP^C to PrP^{Sc}.[30] At the specified interval, aliquots of the incubation solution were taken out and added to the detection system containing Au NC@SiO_2-Apt. Subsequently, BSNVA was added to the above mixture for the following fluorescence measurement. The FL of detection system emitted faintly and remained almost unchanged when incubation time was less than 20 min. After 30 min of incubation, the mixture became emissive and the FL intensity increased rapidly as incubation time went by. The FL intensity reached its maximum at 90 min, after which the fluorescence no longer changed (**Figure 7**).

The results indicate that the transformation for the PrP^C includes a three-step process. The first step represents a lag phase of nucleation. Nucleation is a rate-limiting step in protein conformational changes, during which the β-sheet structure has not been produced due to the absence of seeds. Subsequently, the PrP^C is unstable under acidic conditions and high temperature, which can trigger conformation changes to form a β-sheet-rich form of the PrP^{Sc}. The formation of PrP^{Sc} can in turn promote the conversion of PrP^C to PrP^{Sc}, which rapidly increases the fluorescence of the detection system. This is the second stage that represents the elongation process. Finally, the transformation from PrP^C to PrP^{Sc} reaches an equilibrium stage, and the fluorescence signal of the mixture tends to be stable. The results are consistent with a nucleation-dependent elongation model, in which the three phases correspond to nucleation, extension, and equilibrium phases, respectively.[33] It is worth mentioning that, based on the hydrophobic effect between AIE molecules and proteins, the PEF–AIE sensor is also expected to monitor the conformational changes of other proteins by selecting appropriate aptamers and corresponding proteins.

The FL signals of Au NC@SiO_2-Apt-PrP^{Sc}-BSNVA varying with PrP^{Sc} concentrations are recorded at an excitation wavelength of 410 nm. The emission of Au NC@SiO_2-Apt-PrP^{Sc}-BSNVA increases gradually following the increase of PrP^{Sc} concentration (**Figure 8**A). However, the FL intensity of Au NC@SiO_2-Apt-PrP^C-BSNVA is lower than that of Au NC@SiO_2-Apt-PrP^{Sc}-BSNVA and remains almost unchanged with the change of PrP^C concentration (Figure 8B,C). A good liner relationship with the PrP^{Sc} concentration in the range from 0 to 15×10^{-9} M with R^2 of 0.999 is observed (Figure 8D), and the limit of detection is calculated to be 10 pM (3σ). Compared with the traditional fluorescence assay, which is direct detection of PrP^{Sc} by BSNVA, the sensitivity of this method is higher and improves by 100 times (Figure S11, Supporting Information). In addition, the selectivity of the present strategy for PrP^{Sc} detection has been further confirmed by the comparison of signals obtained in the presence of other proteins, glucides, and some amino acids (Figure S12, Supporting Information). As demonstrated, these interferences have not significantly changed the signal, and thus the PEF–AIE sensor could be further utilized for detecting PrP^{Sc} in human serum sample (Table S1, Supporting Information). The relative standard deviation for 5 nmol L^{-1} PrP^{Sc} was 2.28% (n = 5), and the corresponding recovery is 102.8%. This indicated that the method could be utilized for detecting PrP^{Sc} in real sample.

2.5. Possible Mechanism of the PEF–AIE Sensor

The mechanism of PEF–AIE sensor to monitor the conformational transformation is directly related to the properties of fluorescent molecule and protein structure. The molecule BSNVA itself is non-emissive by annihilating its excited states through phenyl of PEF–AIE sensor torsional motions. Our experimental

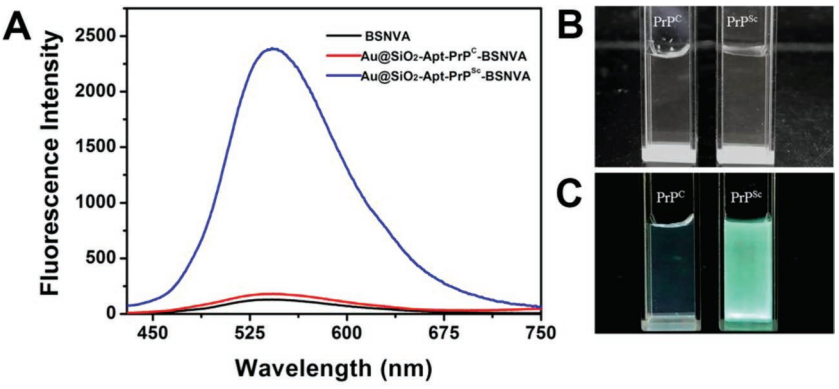

Figure 6. A) FL spectra of Au NC@SiO_2-Apt-PrP^C-BSNVA (red line), Au NC@SiO_2-Apt-PrP^{Sc}-BSNVA (blue line) and BSNVA (black line). Photographs of mixtures of Au NC@SiO_2-Apt-PrP^C-BSNVA and Au NC@SiO_2-Apt-PrP^{Sc}-BSNVA mixtures taken under B) normal laboratory lighting and C) illumination with a UV light of 365 nm.

© 2019 WILEY-VCH Verlag GmbH & Co. KGaA, Weinheim

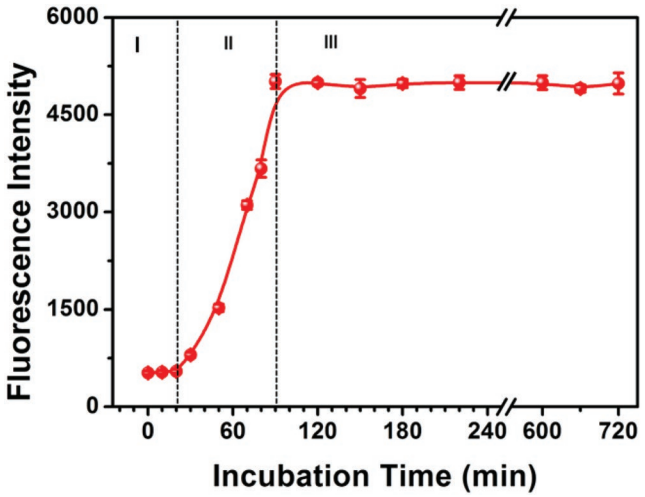

Figure 7. The conformation change process of PrP monitored by Au NC@SiO_2-Apt-PrP^{Sc}-BSNVA sensor.

results clearly show that BSNVA molecule turns to be luminescent in complex with the PrP^{Sc} with obvious AIE character. The experimental results inferred that bound with PrP^{Sc} effectly limits intramolecular motions (RIM) or rotations (RIR) of BSNVA thus switches on the fluorescence emission. However, we also have an interesting observation that the BSNVA remains nearly non-emissive in complex with PrP^{C}, which contains less β-sheet contents in its effector binding site compared with PrP^{Sc}, which prompts us to speculate that the BSNVA specifically recognizes and interacts with β-sheet structure in PrP^{Sc}.

To gain deeper insights into the interactions between BSNVA and PrP and to better understand the binding mechanism, the docking simulations were performed. As shown in **Figure 9**A, PrP^{C} is stable under neutral pH, which contains three well-resolved α-helices (α1, α2, and α3) and almost no β-sheet structure. In contrary to PrP^{C}, the PrP^{Sc} contains two significant β-sheet structures (Figure 9B). The transformation from α-helices to β-sheets structure is a necessary feature in the formation of PrP^{Sc} from PrP^{C}. Our docking results clearly show the preference of BSNVA's affinity to the β-sheet region of PrP^{Sc}. (Figure 9D). In the docked BSNVA-PrP^{Sc} complex, except the hydrophobic interactions between the aromatic rings of BSNVA and the exposed hydrophobic residues (L130 and Y162) from PrP^{Sc}, there are also two hydrogen bonds formed between the oxygen atoms of sulfonate groups of BSNVA and two residues, K194 and L125 from PrP^{Sc}. Whereas in PrP^{C}, the hydrophobic residues that interact with BSNVA in PrP^{Sc} are wrapped in inside into the α-helices. Hence in the docked BSNVA-PrP^{C} complex, only two hydrogen bonds are formed between PrP^{C} and BSNVA molecule (Figure 9C). The loose binding to PrP^{C} thus allows the phenyl groups in BSNVA to be dynamic rotational and renders fluorescence quenching of it. The looser binding between PrP^{C} and BSNVA could also be evidenced from the binding energy. The obtained lowest docking energy between BSNVA and PrP^{C} (–9.40 kcal mol^{-1}) from 500 runs of docking is much higher than that between BSNVA and

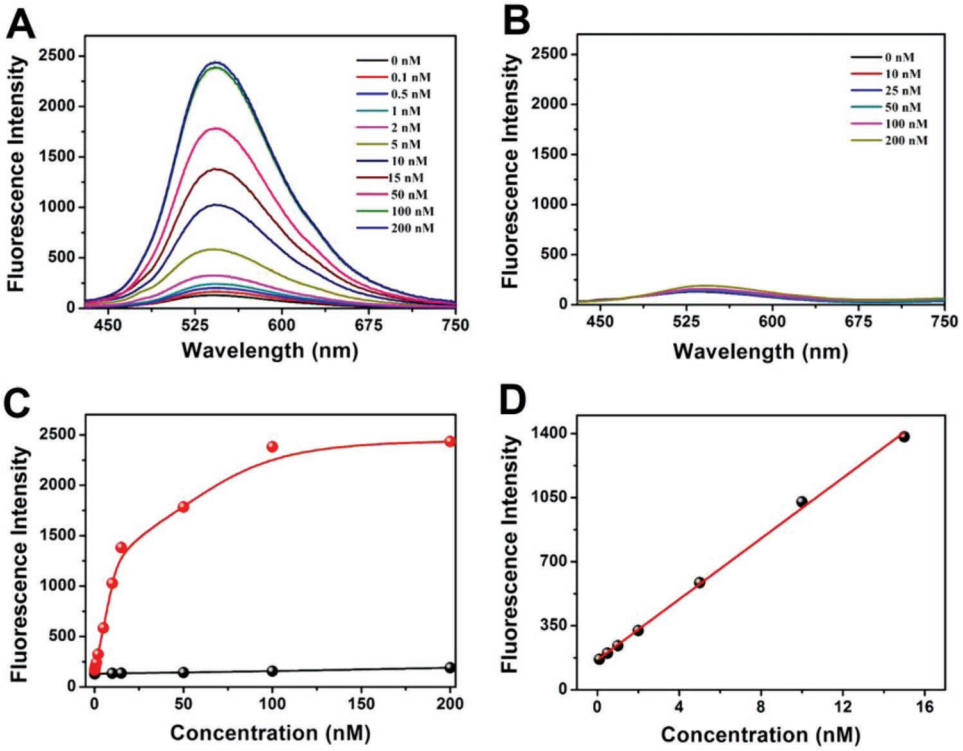

Figure 8. A) FL spectra of Au NC@SiO_2-Apt-PrP^{Sc}-BSNVA complexes upon addition of different concentrations of PrP^{Sc}. B) FL spectra of Au NC@SiO_2-Apt-PrP^{C}-BSNVA complexes upon addition of different concentrations of PrP^{C}. C) FL intensity of PEF–AIE sensor varies with the concentration of PrP^{Sc} (red line) or PrP^{C} (black line). D) The linear relationship between the PrP^{Sc} concentrations and the FL intensity of Au NC@SiO_2-Apt-PrP^{Sc}-BSNVA.

© 2019 WILEY-VCH Verlag GmbH & Co. KGaA, Weinheim

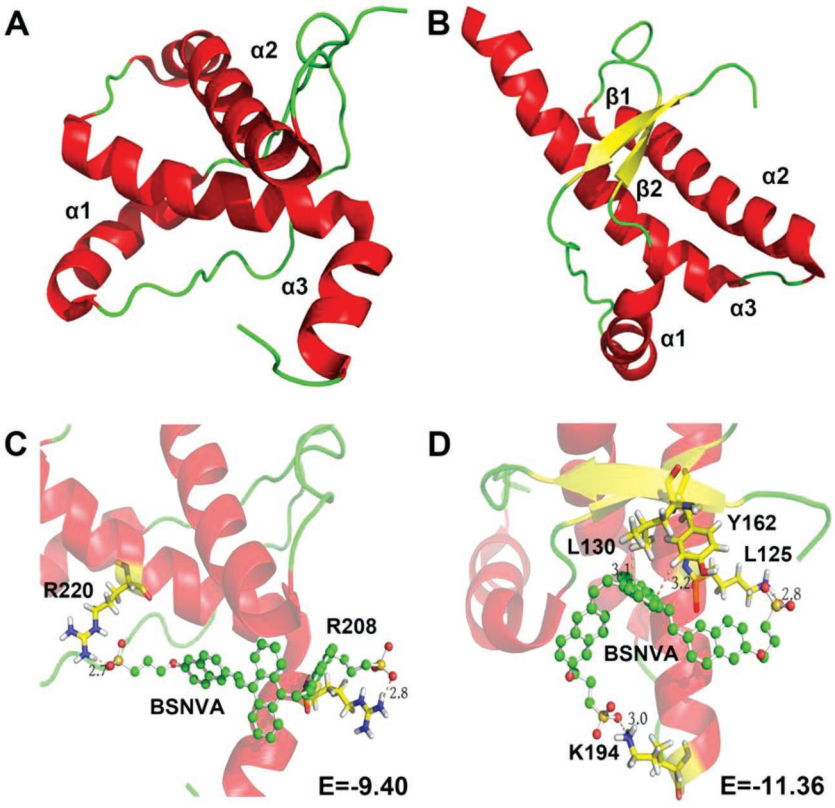

Figure 9. Crystal structures of A) PrP^C and B) PrP^{Sc}. C) The best docked complex between BSNVA and PrP^C with the lowest binding free energies (*E*; kcal mol^{-1}). D) The best docked complex between BSNVA and PrP^{Sc} with the lowest binding free energies (*E*; kcal mol^{-1}). The ligand BSNVA is represented as in ball and stick mode, with carbon, oxygen, and sulfonate atoms colored in green, red, and orange, respectively. The crystal structure of PrP^C and PrP^{Sc} are represented as cartoon, with α-helices, β-sheets, and fibril colored in red, yellow, and green, respectively. The key residues in the crystal structures of PrP^C and PrP^{Sc} are represented with sticks, with carbon, oxygen, and nitrogen atoms colored in yellow, red, and blue, respectively.

PrP^{Sc} (–11.36 kcal mol^{-1}). To further identify the relationship between the binding strength of BSNVA to PrPs and their β-sheet content degree, we choose the other three representative PrP structures (PDB ID: 2K1D, 3HAK, and 1QLX), with different degrees of β-sheets content from low to high, to examine their binding behavior with BSNVA molecule (**Figure 10**). The resulted binding energy of BSNVA to them calculated from docking results are listed in the Table S2 in the Supporting Information. The binding energy of BSNVA to PrP listed in the table displays obvious positive corrleation to the degree of β-sheet contents in PrPs. The preference of the BSNVA to β-sheet structure could also observed from the docked complex structures. In short, the docking simulations confirmed the experiment observation that the BSNVA specifically recognizes and binds to the β-sheet structure in PrPs.

2.6. Method Validation by CD and SEM

CD is a common method for the analysis of protein conformation.[34] To further verify the validity of the above-mentioned results, CD spectroscopy is performed to monitor the secondary structure changes of PrP during the conformational transformation (**Figure 11**). At first, the secondary structure of PrP^C was α-helices, with two negative bands at 207 and 222 nm. There was no significant change in the spectral profile as the incubation time has increased from 0 to 30 min, which corresponded to the initial lag phase for nucleation. Subsequently, an obvious decrease in intensity is observed, indicating that PrP has changed from α-helices to β-sheets. After incubation for 90 min, the CD spectra had changed to a broad negative peak at 218 nm, indicating that the secondary structure was dominated by β-sheet. Since then, the β-sheet-rich structure has remained almost unchanged with the increase of incubation time. The extended β-sheet structure leads the conformers to bind to BSNVA. The changes of secondary structure with incubation time are consistent with the change of FL intensity.

The morphology of the PrP was further observed by SEM. At the first stage, the morphology of PrP molecules was small spherical particles with no apparent aggregation. Then, several PrP molecules were integrated into one oligomer with large size. After 2 h of incubation, a number of fibrils were formed (Figure S13, Supporting Information). The CD and SEM results reveal that the structural change of PrP is the important factor leading to the fluorescence change of PEF–AIE sensor.

3. Conclusion

In conclusion, a label-free AIE-based PEF sensor was successfully constructed to monitor the conformational changes in protein, using PrP as a model. A series of anthracene derivatives were synthesized and a water-soluble sulfonate BSNVA with excellent AIE properties was selected to prepare the PEF–AIE sensor. Using an aptamer of PrP as the bridge, we successfully introduced BSNVA into PEF system. To the best of our knowledge, this is the first PEF sensor to realize the fluorescence enhancement of AIE molecule, which expands the scope of application of PEF. The PEF–AIE sensor emits weakly in the presence of PrP^C and strongly in the presence of PrP^{Sc}, which enables the sensor to distinguish the PrP^{Sc} from PrP^C effectively. Furthermore, the sensor has been successfully applied to quantify PrP^{Sc} and monitor conformational changes of PrP. Compared with immunological methods and direct fluorescence assay, such strategy is more sensitive, selective, and economic because it is signal amplification and does not require fluorescent labeling. The strategy provides a new sight for protein detection and conformational monitoring, which is expected to promote the search of protein-conformational diseases.

© 2019 WILEY-VCH Verlag GmbH & Co. KGaA, Weinheim

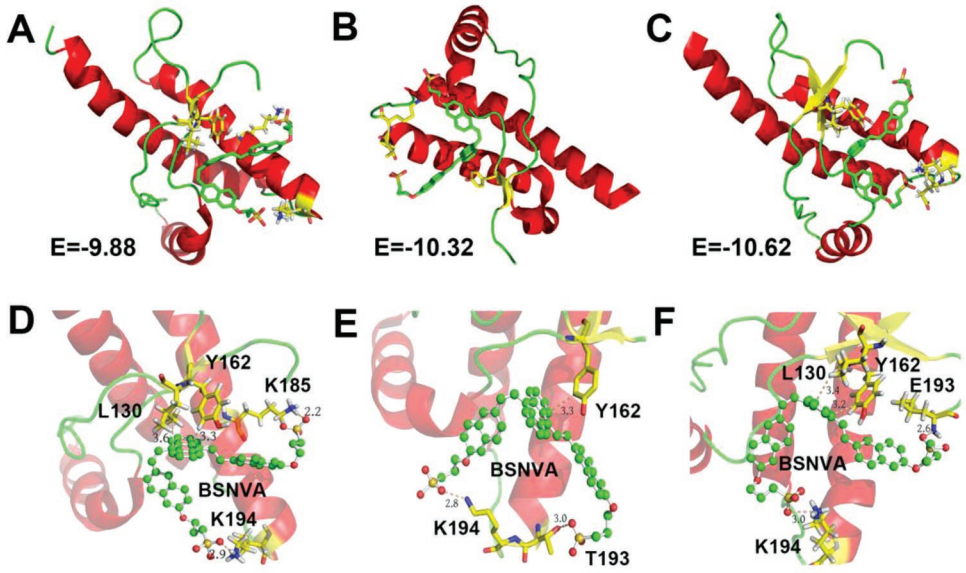

Figure 10. A–C) The docked complexes of BSNVA and PrPs with the lowest binding free energies (*E*; kcal mol^{-1}). D–F) The detailed docked complexes of BSNVA and PrPs with different degrees of the β-sheet content. The ligand BSNVA is represented in ball and stick mode, with carbon, oxygen, and sulfonate atoms colored in green, red, and orange, respectively. The crystal structures of PrP^{C} and PrP^{Sc} are represented as cartoon, with α-helices, β-sheets, and fibril colored in red, yellow, and green, respectively. The key resudies in crystal structures of PrP^{C} and PrP^{Sc} are represented as sticks, with carbon, oxygen, and nitrogen atoms colored in yellow, red, and blue, respectively.

4. Experimental Section

Chemicals and Materials: All reagents were purchased from suppliers without further purification. Anthracene, paraformaldehyde, potassium tert-butoxide (t-BuOK), and (3-Aminopropyl) triethoxysilane (APTES, 98%) were obtained from Alfa Aesar (Shanghai, China). 6-Methoxy-2-naphthaldehyde was purchased from Tokyo Chemical Industry (Shanghai, China). Chloroauric acid hydrated ($HAuCl_4{\cdot}4H_2O$) was obtained from Sinopharm Chemical Reagent Co., Ltd (China). Boron tribromide, THF, dry dichloromethane (DCM), sodium borohydride, hexadecyltrimethylammonium bromide (CTAB), L-Ascorbic acid, tetraethyl orthosilicate, and 2,4,6-trichloro-1,3,5-triazine were purchased from Sigma–Aldrich (Shanghai, China). Triethyl phosphite was get from InnoChem (Beijing, China). Hydrochloric acid, methanol, petroleum ether (PE), sodium chloride, concentrated sulfuric acid were purchased from Beijing Chemical Works. PrP was obtained from Calbiochem (Germany). The amino acid sequence of human PrP is shown in Supporting Information S1. PrP^{Sc} aptamer was synthesized by Sangon Tech. Ltd. (Shanghai, China), and the sequence is shown in Supporting Information S2. Human serum was purchased from Biodee (Beijing, China). Deionized water (18.2 MΩ cm) was purified with a Milli-Q water purification.

Instrumentation: ^{1}H NMR spectra were measured on a JEOL 400 MHz spectrometer using chloroform-d ($CDCl_3$) or dimethyl sulfoxide (DMSO) as solvent. Mass spectral measurements were taken by a Thermo Fisher Scientific LTQ-XL. UV–vis spectra were recorded on UV-2450 spectrometer (Shimadzu, Japan). Fluorescence spectra were measured using a RF-6000 (Shimadzu, Japan). Transmission electron microscopy (TEM) images were measured on a JEOL 2010 transmission electron microscope. The morphology of the products were obtained on an SEM (FESEM, S-8010, Hitachi). The zeta potential measurements were obtained on a Nano-ZS Zetasizer ZEN3600 (Malvern Instruments Ltd, UK). Fluorescence imaging was performed on a confocal laser scanning microscope (Nikon ALR, Japan). CD spectra were recorded on a J-810 spectropolarimeter (JASCO) from 180 to 260 nm.

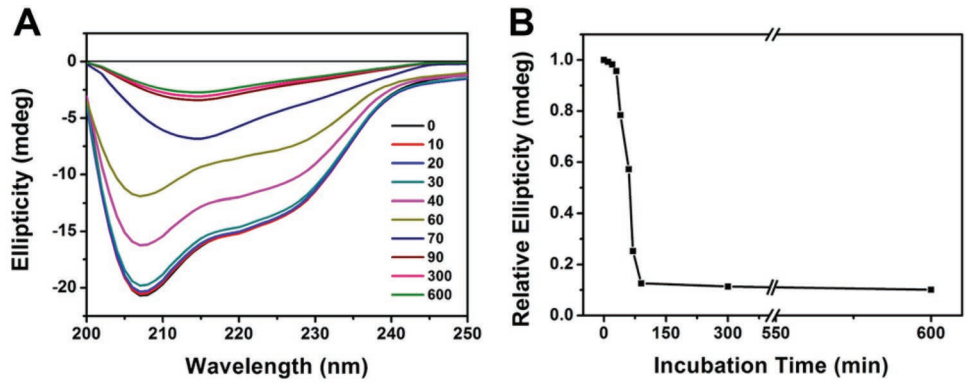

Figure 11. A) CD spectra of PrP in a pH 4 buffer at 65 °C for different periods of time (0–600 min). B) Change of CD spectra intensity at 208 nm with different incubation time.

© 2019 WILEY-VCH Verlag GmbH & Co. KGaA, Weinheim

Synthesis of 9,10-bis[2-(6-methoxy)naphthylethenyl]anthracene (BMNVA): Compounds 1 and 2 were synthesized according to the literature, and the synthetic details are shown in the Supporting Information.[35] Compound 2 (1 g, 2.08 mmol) and t-BuOK (1.2 g, 10.69 mmol) was dissolved in THF (40 mL) under nitrogen. The solution was stirred for 1 h at 0 °C. 6-methoxy-2-naphthaldehyde (1.4 g, 7.52 mmol) in THF (40 mL) was added to the mixture. Then, the mixture was kept at room temperature and stirred for 12 h. The resultant precipitate was washed successively with MeOH and filtered off to give compound as yellow powder (56.68% yield). ^{1}H NMR (400 MHz, $CDCl_3$) δ 8.47 (dd, J = 6.8, 3.3 Hz, 4H), 8.03 (d, J = 16.4 Hz, 2H), 7.96–7.78 (m, 8H), 7.50 (dd, J = 6.9, 3.2 Hz, 4H), 7.19 (d, J = 8.2 Hz, 4H), 7.09 (d, J = 16.5 Hz, 2H), 3.97 (s, 6H); m/z 543.23 $[M + H]^+$; and elemental analysis calcd (%) for $C_{40}H_{30}O_2$: C 88.53, H 5.57,O 5.90; found: C 88.51, H 5.58, and O 6.92.

Synthesis of 9,10-bis[2-(6-hydroxy)naphthylethenyl]anthracene (BHNVA): Compound 3 (0.4066 g, 1 mmol) and dry DCM (10 mL) were added into a 50 mL three-necked bottle. The mixture was kept in liquid nitrogen-ethanol at −78 °C. Boron tribromide (3 mL, 1 M) in CH_2Cl_2 solution was added carefully to the mixture while stirring. Then, the mixture was stirred for 12 h and allowed to gradually return to room temperature. Subsequently, 10 mL water was added carefully to the mixture and stirred for 30 min to make the product and unreacted boron tribromide hydrolyze. After that, the mixture was extracted with DCM, the organic phase was washed with brine, dried with $MgSO_4$ and concentrated with to dryness under vacuum. Finally, the crude product was chromatographed over silica gel. The column was eluted with a mixture (3:2) of PE and acetone to yield 0.52 g (69%) of a yellow powder. ^{1}H NMR (400 MHz, DMSO) δ 9.84 (s, 2H), 8.44 (dd, J = 6.8, 3.3 Hz, 4H), 8.18 (d, J = 16.5 Hz, 2H), 8.09–7.99 (m, 4H), 7.79 (dd, J = 8.7, 4.2 Hz, 4H), 7.57 (dd, J = 6.9, 3.2 Hz, 4H), 7.18 (d, J = 2.2 Hz, 2H), 7.11 (dd, J = 8.7, 2.3 Hz, 2H), 7.04 (d, J = 16.4 Hz, 2H). m/z = 515.23 $[M + H]^+$; and elemental analysis calcd (%) for $C_{38}H_{26}O_2$: C 88.69, H 5.09, O 6.22; found: C 90.01, H 5.58, and O 6.92.

Synthesis of 9,10-bis[2-(6-sulfonatopropoxyl)naphthylethenyl]anthracene (BSNVA): Compound 4 (0.515 g, 1 mmol) and 20 mL of anhydrous ethanol were added into 100 mL three-necked bottle under nitrogen. Then a solution of NaOEt (0.1565 g, 2.3 mmol) in anhydrous ethanol (20 mL) was added by dropwise to the above mixture and stirred until the solution color turned to orange–red. Subsequently, 1,3-propanesultone (200 µL) in ethanol (20 mL) was added to the reaction mixture. The mixture was vigorously stirred overnight and a yellow product was precipitated out from the solution. Finally, the product was filtrated and then washed with ethanol and acetone two times to give g of a yellow powder. ^{1}H NMR (400 MHz, DMSO) δ 8.46 (dd, J = 6.8, 3.3 Hz, 4H), 8.19 (d, J = 16.5 Hz, 2H), 8.10–8.02 (m, 4H), 7.81 (dd, J = 8.7, 5.0 Hz, 4H), 7.58 (dd, J = 6.9, 3.2 Hz, 4H), 7.21–7.10 (m, 4H), 7.06 (d, J = 16.5 Hz, 2H), 4.07 (t, J = 6.5 Hz, 4H), 2.63 (t, J = 7.4 Hz, 4H), 2.02–1.97 (m, 4H). ^{13}C NMR (126 MHz, DMSO) δ 156.25, 138.02, 134.95, 132.93, 131.94, 130.14, 129.52, 128.30, 127.31, 127.09, 126.78, 126.04, 124.50, 124.02, 119.51, 109.43, 67.24, 49.11, and 25.31. m/z = 378.07 $[M\text{-}2Na]^{2-}$, and elemental analysis calcd (%) for $C_{44}H_{36}Na_2O_8S_2$: C 65.82, H 4.52, Na 5.73, O 15.94, S 7.99; found: C 65.84, H 4.49, Na 5.73, O 15.96, and S 7.98.

Fabrication of PEF Sensor: According to the literature and the previous work, core–shell Au NC@SiO_2 NPs were prepared.[14d] The detailed information about the immobilization of aptamer onto Au NC@SiO_2 NPs (Au NC@SiO_2-Apt, ASA) is located in the Supporting Information. It is worth noting that, in order to ensure the stability of ASA, the prepared samples need to be used as soon as possible. The formation of Au NC@SiO_2-Apt-PrP^{Sc}–BSNVA NPs followed the schematic diagram in Scheme 1. In short, 1 mL of ASA NPs solution with a certain concentration was first mixed with the PrP^{Sc} in varied concentrations. Then, the mixtures were incubated at 4 °C for 30 min. During this procedure, PrP^{Sc} was specifically captured by ASA NPs. After that, the suspensions were collected via centrifugation. The concentrated Au NC@SiO_2-Apt-PrP^{Sc} conjugates were redispersed in the phosphate buffer saline (PBS) buffer via gentle shaking. Finally, BSNVA was added to the dispersed Au NC@SiO_2-Apt-PrP^{Sc} solution.

PEF–AIE Sensor for Monitoring Conformational Changes of PrP: PrP^C was dissolved in a sodium acetate-acetic acid buffer (pH 4.0) and incubated at 65 °C to achieve the transformation from PrP^C to PrP^{Sc}. An aliquot of the PrP^C solution taken out from the incubation mixture at a defined time and added to the detection system containing Au NC@SiO_2-Apt. Subsequently, BSNVA was added to the above mixture for the following fluorescence measurement. The final concentration of PrP and BSPOTPE were both 5×10^{-6} M.

Calculation Details: The geometry structure of the ligand BSNVA molecule was optimized by density functional theory (DFT) method B3LYP functional with 6–31G(d) basis set. Five representative conformations of human PrP which present different degrees of β-sheet content(PDB ID: 2K1D, 1HJM, 3HAK, 1QLX, and 1HJN) were chosen to investigate their interaction with BSNVA. In order to establish the complex model, BSNVA was first docked into the human PrP structures by using AutoDock 4.2 software package with the AutoDock Lamarckian Genetic algorithm.[36] The proteins were all kept to be rigid in the docking process, while the ligand BSNVA was set to be rotatable bonds to allow it to better fit in the pocket. A default docking parameters were applied. All the docking simulations were performed for 500 runs.

Supporting Information

Supporting Information is available from the Wiley Online Library or from the author.

Acknowledgements

J.O. gratefully acknowledges the support from the National Natural Science Foundation of China (21675014 and 21475011) and the Fundamental Research Funds for the Central Universities. H.T. gratefully acknowledges the support from the National Natural Science Foundation of China (21571019). N.N. gratefully acknowledges the support from the National Natural Science Foundation of China (21675015).

Conflict of Interest

The authors declare no conflict of interest.

Keywords

aggregation-induced emission, fluorescence sensor, plasmonic enhancement, prion protein, protein conformation

Received: October 12, 2018
Revised: December 21, 2018
Published online:

[1] a) S. L. Bernstein, N. F. Dupuis, N. D. Lazo, T. Wyttenbach, M. M. Condron, G. Bitan, D. B. Teplow, J. Shea, B. T. Ruotolo, C. V. Robinson, M. T. Bowers, *Nat. Chem.* **2009**, *1*, 326; b) C. M. Dobson, *Nature* **2003**, *426*, 884; c) R. Kayed, E. Head, J. L. Thompson, T. M. McIntire, S. C. Milton, C. W. Cotman, C. G. Glabe, *Science* **2003**, *300*, 486.

[2] a) A. Ahmad, V. N. Uversky, D. Hong, A. L. Fink, *J. Biol. Chem.* **2005**, *280*, 42669; b) N. Rubin, E. Perugia, M. Goldschmidt, M. Fridkin, L. Addadi, *J. Am. Chem. Soc.* **2008**, *130*, 4602; c) N. K. Mishra, K. B. Joshi, S. Verma, *Mol. Pharmaceutics* **2013**, *10*, 3903; d) C. L. Teoh, D. Su, S. Sahu, S. W. Yun, E. Drummond, F. Prelli,

© 2019 WILEY-VCH Verlag GmbH & Co. KGaA, Weinheim

S. Lim, S. Cho, S. Ham, T. Wisniewski, Y. T. Chang, *J. Am. Chem. Soc.* **2015**, *137*, 13503; e) D. Etezadi, J. B. Warner Iv, F. S. Ruggeri, G. Dietler, H. A. Lashuel, H. Altug, *Light: Sci. Appl.* **2017**, *6*, 17029; f) J. A. Jackman, A. R. Ferhan, B. K. Yoon, J. H. Park, V. P. Zhdanov, N. J. Cho, *Anal. Chem.* **2017**, *89*, 12976; g) J. H. Park, J. A. Jackman, A. R. Ferhan, G. J. Ma, B. K. Yoon, N. J. Cho, *ACS Appl. Mater. Interfaces* **2018**, *10*, 32047.

[3] a) Y. Liu, K. Ai, X. Cheng, L. Huo, L. Lu, *Adv. Funct. Mater.* **2010**, *20*, 951; b) X. Lim, *Nature* **2016**, *531*, 26.

[4] a) M. Groenning, *J. Chem. Biol.* **2010**, *3*, 1; b) P. Hammarstrom, R. Simon, S. Nystrom, P. Konradsson, A. Aslund, K. P. Nilsson, *Biochemistry* **2010**, *49*, 6838; c) C. Rodriguez-Rodriguez, A. Rimola, L. Rodriguez-Santiago, P. Ugliengo, A. Alvarez-Larena, H. Gutierrez-de-Teran, M. Sodupe, P. Gonzalez-Duarte, *Chem. Commun.* **2010**, *46*, 1156.

[5] Y. Hong, L. Meng, S. Chen, C. W. Leung, L. T. Da, M. Faisal, D. A. Silva, J. Liu, J. W. Lam, X. Huang, B. Z. Tang, *J. Am. Chem. Soc.* **2012**, *134*, 1680.

[6] a) M. Kumar, Y. Hong, D. C. Thorn, H. Ecroyd, J. A. Carver, *Anal. Chem.* **2017**, *89*, 9322; b) R. Khurana, V. N. Uversky, L. Nielsen, A. L. Fink, *J. Biol. Chem.* **2001**, *276*, 22715; c) M. Groenning, L. Olsen, M. van de Weert, J. M. Flink, S. Frokjaer, F. S. Jorgensen, *J. Struct. Biol.* **2007**, *158*, 358.

[7] a) Y. Gao, G. Feng, T. Jiang, C. Goh, L. Ng, B. Liu, B. Li, L. Yang, J. Hua, H. Tian, *Adv. Funct. Mater.* **2015**, *25*, 2857; b) C. L. Chiang, S.-M. Tseng, C. T. Chen, C. P. Hsu, C. F. Shu, *Adv. Funct. Mater.* **2008**, *18*, 248.

[8] J. Luo, Z. Xie, J. W. Y. Lam, L. Cheng, B. Z. Tang, H. Chen, C. Qiu, H. S. Kwok, X. Zhan, Y. Liu, D. Zhu, *Chem. Commun.* **2001**, *18*, 1740.

[9] a) L. Zhang, N. He, C. Lu, *Anal. Chem.* **2015**, *87*, 1351; b) J. Mei, Y. Hong, J. W. Lam, A. Qin, Y. Tang, B. Z. Tang, *Adv. Mater.* **2014**, *26*, 5429.

[10] Q. Qi, J. Qian, S. Ma, B. Xu, S. X. Zhang, W. Tian, *Chem. – Eur. J.* **2015**, *21*, 1149.

[11] a) G. R. Kumar, S. K. Sarkar, P. Thilagar, *Chem. – Eur. J.* **2016**, *22*, 17215; b) M. Kang, X. Gu, R. T. Kwok, C. W. Leung, J. W. Lam, F. Li, B. Z. Tang, *Chem. Commun.* **2016**, *52*, 5957; c) C. Felip-Leon, F. Galindo, J. F. Miravet, *Nanoscale* **2018**, *10*, 17060; d) M. Gao, B. Z. Tang, *ACS Sens.* **2017**, *2*, 1382; e) X. Wang, J. Dai, X. Min, Z. Yu, Y. Cheng, K. Huang, J. Yang, X. Yi, X. Lou, F. Xia, *Anal. Chem.* **2018**, *90*, 8162.

[12] Y. Hong, C. Feng, Y. Yu, J. Liu, J. W. Y. Lam, K. Q. Luo, B. Z. Tang, *Anal. Chem.* **2010**, *82*, 7035.

[13] a) B. Sun, X. Yang, L. Ma, C. Niu, F. Wang, N. Na, J. Wen, J. Ouyang, *Langmuir* **2013**, *29*, 1956; b) C. W. Leung, F. Guo, Y. Hong, E. Zhao, R. T. Kwok, N. L. Leung, S. Chen, N. N. Vaikath, O. M. El-Agnaf, Y. Tang, W. P. Gai, B. Z. Tang, *Chem. Commun.* **2015**, *51*, 1866.

[14] a) L. Liang, F. Lan, S. Ge, J. Yu, N. Ren, M. Yan, *Anal. Chem.* **2017**, *89*, 3597; b) X. Ji, C. Xiao, W. F. Lau, J. Li, J. Fu, *Biosens. Bioelectron.* **2016**, *82*, 240.

[15] a) Y. Kim, B. Kang, H. Y. Ahn, J. Seo, K. T. Nam, *Small* **2017**, *13*, 1700071; b) S. Xu, L. Jiang, Y. Nie, J. Wang, H. Li, Y. Liu, W. Wang, G. Xu, X. Luo, *ACS Appl. Mater. Interfaces* **2018**, *10*, 26851.

[16] a) L. Wang, Q. Song, Q. Liu, D. He, J. Ouyang, *Adv. Funct. Mater.* **2015**, *25*, 7017; b) C. Niu, Q. Song, G. He, N. Na, J. Ouyang, *Anal. Chem.* **2016**, *88*, 11062; c) Q. Song, M. Peng, L. Wang, D. He, J. Ouyang, *Biosens. Bioelectron.* **2016**, *77*, 237; d) Y. Cui, C. Niu, N. Na, J. Ouyang, *J. Mater. Chem. B* **2017**, *5*, 5329.

[17] a) D. Wang, H. Su, R. T. K. Kwok, X. Hu, H. Zou, Q. Luo, M. M. S. Lee, W. Xu, J. W. Y. Lam, B. Z. Tang, *Chem. Sci.* **2018**, *9*, 3685; b) X. Lou, Y. Zhuang, X. Zuo, Y. Jia, Y. Hong, X. Min, Z. Zhang, X. Xu, N. Liu, F. Xia, B. Z. Tang, *Anal. Chem.* **2015**, *87*, 6822.

[18] X. He, Z. Zhao, L. H. Xiong, P. F. Gao, C. Peng, R. S. Li, Y. Xiong, Z. Li, H. H. Sung, I. D. Williams, R. T. K. Kwok, J. W. Y. Lam, C. Z. Huang, N. Ma, B. Z. Tang, *J. Am. Chem. Soc.* **2018**, *140*, 6904.

[19] a) N. Song, D. X. Chen, M. C. Xia, X. L. Qiu, K. Ma, B. Xu, W. Tian, Y. W. Yang, *Chem. Commun.* **2015**, *51*, 5526; b) H. Wang, K. Ma, B. Xu, W. Tian, *Small* **2016**, *12*, 6613.

[20] a) F. Wang, J. Wen, L. Huang, J. Huang, J. Ouyang, *Chem. Commun.* **2012**, *48*, 7395; b) C. Niu, Y. You, L. Zhao, D. He, N. Na, J. Ouyang, *Chem. – Eur. J.* **2015**, *21*, 13983.

[21] J. Zhang, S. Ma, H. Fang, B. Xu, H. Sun, I. Chan, W. Tian, *Mater. Chem. Front.* **2017**, *1*, 1422.

[22] C. Niu, L. Zhao, T. Fang, X. Deng, H. Ma, J. Zhang, N. Na, J. Han, J. Ouyang, *Langmuir* **2014**, *30*, 2351.

[23] M. Wang, G. Hartmann, Z. Wu, L. Scarabelli, B. B. Rajeeva, J. W. Jarrett, E. P. Perillo, A. K. Dunn, L. M. Liz-Marzan, G. S. Hwang, Y. Zheng, *Small* **2017**, *13*, 1701763.

[24] M. Li, S. K. Cushing, N. Wu, *Analyst* **2015**, *140*, 386.

[25] N. Gandra, C. Portz, L. Tian, R. Tang, B. Xu, S. Achilefu, S. Singamaneni, *Angew. Chem., Int. Ed.* **2014**, *53*, 866.

[26] T. T. Zhao, K. Yu, L. Li, T. S. Zhang, Z. P. Guan, N. Y. Gao, P. Y. Yuan, S. Li, S. Q. Yao, Q. H. Xu, G. Q. Xu, *ACS Appl. Mater. Interfaces* **2014**, *6*, 2700.

[27] E. Biasini, J. A. Turnbaugh, U. Unterberger, D. A. Harris, *Trends Neurosci.* **2012**, *35*, 92.

[28] W. Q. Zou, J. Zheng, D. M. Gray, P. Gambetti, S. G. Chen, *Proc. Natl. Acad. Sci. USA* **2004**, *101*, 1380.

[29] G. S. Jackson, L. L. Hosszu, A. Power, A. F. Hill, J. Kenney, H. Saibil, C. J. Craven, J. P. Waltho, A. R. Clarke, J. Collinge, *Science* **1999**, *283*, 1935.

[30] Z. Lou, J. Wan, X. Zhang, H. Zhang, X. Zhou, S. Cheng, N. Gu, *Colloids Surf., B* **2017**, *157*, 31.

[31] X. Ma, H. Graig, Benson, M. Debbie, J. M. Aiken, J. A. Pedersen, *Environ. Sci. Technol.* **2007**, *41*, 2324.

[32] D. O. V. Alonso, C. An, V. Daggett, *Phil. Trans. R. Soc. London. Ser. A: Math. Phys. Eng. Sci.* **2002**, *360*, 1165.

[33] K. I. Yamaguchi, K. Kuwata, *Biophys. Rev.* **2018**, *10*, 517.

[34] G. Qin, M. J. Glassman, C. N. Lam, D. Chang, E. Schaible, A. Hexemer, B. D. Olsen, *Adv. Funct. Mater.* **2015**, *25*, 729.

[35] Y. Dong, B. Xu, J. Zhang, X. Tan, L. Wang, J. Chen, H. Lv, S. Wen, B. Li, L. Ye, B. Zou, W. Tian, *Angew. Chem., Int. Ed.* **2012**, *51*, 10782.

[36] a) G. M. Morris, D. S. Goodsell, R. S. Halliday, R. Huey, W. E. Hart, R. K. Belew, A. J. Olson, *J. Comput. Chem.* **1998**, *19*, 1639; b) G. M. Morris, R. Huey, W. Lindstrom, M. F. Sanner, R. K. Belew, D. S. Goodsell, A. J. Olson, *J. Comput. Chem.* **2009**, *30*, 2785.

© 2019 WILEY-VCH Verlag GmbH & Co. KGaA, Weinheim